The Modular Structure of SIP Facilitates Its Role in Stabilizing Multiprotein Assemblies[†,‡]

Shibani Bhattacharya,[§,||] Young-Tae Lee,[§,||] Wojciech Michowski,[⊥] Beata Jastrzebska,[⊥] Anna Filipek,[⊥] Jacek Kuznicki,[⊥,@] and Walter J. Chazin*[,§,#]

Departments of Biochemistry and Physics, Center for Structural Biology, 5140 BIOSCI/MRBIII, Vanderbilt University, Nashville, Tennessee 37232-8725, Department of Molecular and Cellular Neurobiology, Nencki Institute of Experimental Biology, 02-293 Warsaw, Poland, and International Institute of Molecular and Cell Biology, Trojdena 4, Warsaw, Poland

Received February 14, 2005; Revised Manuscript Received May 13, 2005

ABSTRACT: Siah-interacting protein (SIP) was identified as a novel adaptor that physically links the E3 ubiquitin ligase activity of Siah-1 with Skp1 and Ebi F-Box protein in the degradation of β-catenin, a transcriptional activator of TCF/LEF genes. In this study, we have used solution NMR spectroscopy to characterize the domain structure of SIP, which includes a novel helical hairpin domain at the N-terminus flexibly linked to a CS domain and an unstructured carboxy terminal SGS domain. These studies have been complemented by mapping the sites of functionally important protein−protein interactions involving Siah-1 and Skp1 to individual domains of SIP. NMR-based chemical shift perturbation assays show that Siah-1 interacts with the flexible linker between SIP N and CS domains. This site for interaction in the linker does not perturb residues in the structured region at the N-terminus but does appear to restrict the rotational freedom of the SIP CS domain in the context of the full-length protein. In contrast, Skp1 engages the SIP CS domain exclusively through weak interactions that are not coupled to the other domains. The principal role of the modular structure of SIP appears to be in bringing these two proteins into physical proximity and orchestrating the orientation required for polyubiquitination of β-catenin in the intact SCF-type complex.

Ubiquitin-dependent proteolysis pathways play a crucial role in regulating the cell cycle, proliferation, and differentiation (*19*). These regulatory pathways employ a complex assembly of proteins built around the catalytic activities of ubiquitination enzymes to recruit and process various substrates for degradation in the proteosome (*43*). Some of the most important substrates include a variety of transcription factors whose activity is tightly regulated through degradation and modification by ubiquitin and small ubiquitin-like molecules (*8*). A crucial cellular target is β-catenin, which associates with TCF−LEF transcription factors in the nucleus (*6*) and triggers the expression of cell cycle proteins such as cyclin D1 (*48*), c-myc (*17*), and metalloproteinases (*4*). Since β-catenin is readily transported into the nucleus, resulting in aberrant transcriptional activity of the TCF−LEF complex, multiple ubiquitination pathways regulate its cytosolic levels, including Wnt signaling (reviewed in ref *42*), FLIP inhibition of Fas signaling (*38*), activity of retinoid X receptor (*52*), and a fourth mechanism triggered in response to p53-dependent expression of the E3 ligase Siah-1 (*35*). There is very strong evidence to support the role of disabling these pathways in the onset of various cancers (*32*, *36*).

Siah-1 is a conserved E3 ligase and a homologue of *Drosophila* seven in absentia gene (Sina)[1] required for the degradation of the transcriptional repressor Tramtrack during R7 photoreceptor development (*26*). In humans, the promoter of Siah-1 gene expression is a target of p53 transcriptional activity and hence of interest in tumor suppression (*14*, *29*, *31*, *34*, *35*). The Siah-1 degradation pathway has attracted special attention because it provides a mechanism for eliminating β-catenin that is independent of its state of phosphorylation (*35*). The significance of the Siah-1 pathway is underscored by its ability to target mutant β-catenin overlooked by canonical phosphorylation-dependent Wnt signaling (*44*).

The molecular architecture of the Siah-1 E3 ubiquitin ligase activity in β-catenin degradation is complex. The core

[†]This work was supported by Grants RO1 GM62112 and RO3 TW00136005 from the National Institutes of Health (NIH) and by support for facilities from by the Vanderbilt-Ingram Cancer Center (NIH Grant P30ES00267) and the Vanderbilt Center in Molecular Toxicology (NIH Grant P30CA68485). Additional funds were provided to A.F. by Polish State Committee of Scientific Research Grant 3 P04A 043 22.

[‡] Coordinates for SIP(1−55) have been deposited in the Protein Data Bank as entry 1YSM.

* To whom correspondence should be addressed: Center for Structural Biology, 5140 BIOSCI/MRBIII, Vanderbilt University, Nashville, TN 37232-8725. Telephone: (615) 936-2210. Fax: (615) 936-2211. E-mail: walter.chazin@vanderbilt.edu.

[§] Department of Biochemistry, Center for Structural Biology, Vanderbilt University.

[||] These authors have contributed equally to this work.

[⊥] Nencki Institute of Experimental Biology.

[@] International Institute of Molecular and Cell Biology.

[#] Department of Physics, Vanderbilt University.

[1] Abbreviations: APC, *Adenomatous polyposis coli*; CS, CHORD and Sgt1; Sina, seven in abstentia; Siah, seven in abstentia homologue; SIP, Siah interacting protein; SCF, Skp1-Cullin-1-F-Box; TCF/LEF, T cell factor/lymphoid enhancer factor.

10.1021/bi0502689 CCC: $30.25
Published on Web 06/16/2005

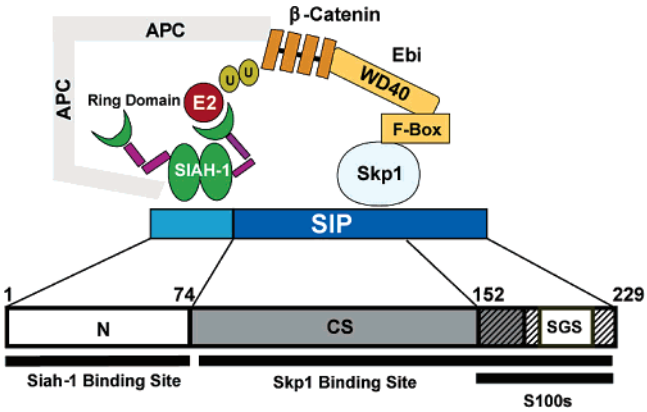

FIGURE 1: Schematic diagram of the Siah-1−SIP−Skp1−Ebi ubiquitination complex. Shown below is the domain organization of SIP and sites of protein−protein interactions. Residues contained within each domain of SIP are labeled.

of the complex is formed by a novel Cullin-1-like adaptor protein SIP, which provides a physical link between the RING domain of Siah-1 and the substrate engaged by the Skp1/Ebi F-Box protein (Figure 1). β-Catenin is specifically recognized by the WD-40 repeat domain of the F-Box protein Ebi and poised for the transfer of ubiquitin from the E2 ligase Ubc-H5/H9 positioned by the RING domain of Siah-1. APC plays an important stabilizing role in this complex through interactions with both Siah-1 and β-catenin (*34*).

The focus of this study is to elucidate the structural role of SIP in the assembly of the Siah-1-mediated E3 ligase complex (*35*). Sequence analysis of the 229-residue SIP protein revealed three distinct regions (Figure 1). The amino acid sequence of the N-terminal region (residues 1−77) displays novel features with some predicted coiled-coil propensity. Although little is known about the structure of this region, it is crucial for interactions with Siah-1 (*35*). The N-terminal region is followed by a CS domain (residues 74−178), which is fused to a SGS domain (residues 152−229). Functionally, SIP(74−229) has been implicated in interactions with Skp1 (*35*), which implies SIP bridges the E2-presenting protein Siah-1 with the substrate binding protein Ebi (Figure 1).

Independent studies by Kuznicki and co-workers (*11*, *13*) have identified the SGS domain as a site for interactions with calcium binding EF-hand proteins belonging to the S100 family. It has been hypothesized that S100 proteins regulate the cellular localization of SIP to the perinuclear region in a phosphorylation-dependent manner (*12*, *51*). However, the phosphorylation of SIP has no clearly defined role in β-catenin degradation (*35*).

This report describes the characterization of the modular structure of SIP and an analysis of the network of protein−protein interactions that are important for its function. Solution NMR techniques have been used to characterize the structure of the three domains of SIP in isolation and the extent of coupling in the intact protein. Chemical shift perturbation assays were applied to map the SIP binding sites for Siah-1 and Skp1. These results provide for the first time structural details of the multiple sites of protein−protein interactions on SIP and insight into the dynamic mechanism that drives the formation of the Siah-1 E3 ubiquitin ligase complex.

MATERIALS AND METHODS

Protein Expression and Purification. Expression systems for intact mouse SIP (residues 1−229) and SIP fragments (residues 1−77, 74−178, 178−229, 155−229, and 73−229) were subcloned from mouse cDNA into the pET28a vector (Novagen), which produces six-His tag fusion proteins separated by a thrombin cleavage site. The gene for human Skp1 was a gift from R. Y. Poon (Hong Kong University) and subcloned into a pET28a vector. The gene for mouse Siah-1 (residues 90−282) was subcloned into a pSV278 plasmid (L. Mizoue, Center for Structural Biology, Vanderbilt University), which produces a MBP fusion-tagged protein with an N-terminal His tag. The proteins were overexpressed in *Escherichia coli* strain BL21(DE3) cells and purified on Ni−NTA resin (Qiagen). The N-terminal His tag or MBP fusion tag was removed by thrombin cleavage followed by separation of products over Ni−NTA resin and a MonoQ column. ^{15}N-enriched and ^{15}N- and ^{13}C-enriched proteins were produced in the same manner using minimal medium containing [$^{13}C_6$]glucose and $^{15}NH_4Cl$ as the sole carbon and nitrogen sources, respectively.

Affinity Chromatography. Affinity resin prepared by coupling intact Skp1 to CNBr−Sepharose beads was equilibrated with buffer containing 20 mM Tris-HCl and 1 mM PMSF at pH 7.5 in microcentrifuge tubes (*11*). Purified fragments of SIP (5−10 μg) were dissolved in the equilibration buffer and incubated with the affinity resin for 15 min at room temperature. The unbound fraction was removed by centrifugation, and the resin was washed five times with the aforementioned buffer. Bound proteins were then eluted from the affinity resin with a buffer containing 0.5 M NaCl. The competitive binding assays were performed using a similar protocol by using SIP-conjugated beads and including 1 mM $CaCl_2$ or 2 mM EGTA in the incubation buffer. In all experiments, the eluant was analyzed by SDS−PAGE and Western blots.

NMR Samples. Unlabeled and ^{15}N-enriched samples of intact SIP, various SIP fragments (residues 1−77, 74−178, and 178−229), and Skp1 were prepared in 20 mM NaP_i and 50 mM NaCl at pH 7.0 in a 90% H_2O/10% D_2O mixture. Additional samples of ^{13}C- and ^{15}N-enriched SIP(1−77) and SIP(74−178) were prepared under identical buffer conditions in a 90% H_2O/10% D_2O mixture or 100% D_2O. The protein concentration in the various samples used for acquiring multidimensional NMR data was determined from the UV absorbance at 280 nm and ranged from 1 to 2 mM.

NMR Resonance Assignments. NMR data were acquired at 303 K on Bruker *AVANCE* 600 and 800 MHz spectrometers and then processed and analyzed using Felix 2000.1 (Accelrys Inc.). The backbone and side chain chemical shifts of SIP(1−77) were assigned using three-dimensional (3D) HNCA, 3D HN(CO)CA, 3D HNCACB, 3D CBCA(CO)NH, 3D HNCO, 3D HC(C)(CO)NH, 3D (H)CC(CO)NH, 3D TOCSY-HSQC, 3D HCCH-TOCSY, two-dimensional (2D) ^{1}H−^{1}H TOCSY, and 2D ^{1}H−^{1}H DQF-COSY experiments (reviewed in refs *5*, *37*, and *46*). With the exception of M1, Q51, and the last three residues at the C-terminal tail (K75, I76, and S77), the backbone was completely assigned as well as more than 95% of the side chain chemical shifts. φ angles were measured from $^3J_{N\alpha}$ and χ_1 angles from $^4J_{N\beta}$ coupling constants extracted from 3D HNHA and 3D HNHB experi-

Table 1: Structural Statistics for the Structure of the SIP N Domain (residues 1−55)

total no. of constraints	999
no. of intraresidue constraints	340
no. of sequential constraints	200
no. of medium-range constraints	320
no. of long-range constraints	49
no. of φ/ψ constraints	74
no. of χ_1 constraints	16

Average Energy and Restraint Violations

⟨distance⟩		⟨angle⟩		⟨energy⟩ (kcal/mol)	
$d > 0.2$ Å	0.0	$\theta > 5°$	0.0	E_{Amber}	-758 ± 16
0.1 Å $< d <$ 0.2 Å	0.25	$\theta < 5°$	0.05	$E_{constraint}$	0.8 ± 0.3
$d <$ 0.1 Å	1.4			$E_{Lennard-Jones}$	-263 ± 5
$\langle d_{max} \rangle$	0.06	$\langle \theta_{max} \rangle$	0.13		

Precision (rmsd)

	backbone (Å)	heavy atoms (Å)
SIP N (residues 3−46)	0.47	1.17
helix I (residues 3−20)	0.22	0.89
helix II (residues 28−46)	0.23	0.97

ments, respectively (*2*). Methyl group stereospecific assignments were obtained from a $^{13}C-^{1}H$ HSQC spectrum acquired on a 10% ^{13}C-labeled sample (*39*). Stereospecific assignments for Hβ protons were obtained from the analysis of $^{3}J_{\alpha\beta}$ coupling constants extracted from a 3D HACAHB-COSY experiment (*16*). Distance restraints used for structure calculations were derived from 3D ^{15}N-edited NOESY-HSQC and 3D ^{13}C-edited NOESY-HSQC experiments.

The backbone chemical shifts of the SIP CS domain (95 of 103 residues, two Pro residues) were assigned using 3D HNCACB and 3D CBCA(CO)NH experiments. At neutral pH, cross-peaks from eight residues at the unstructured C-terminal end are exchange broadened. They were observed in spectra acquired at only pH 4.5.

Perturbation Assay. All NMR experiments were performed using a Bruker *AVANCE* 600 MHz spectrometer equipped with a CryoProbe. For analyzing interactions with Siah-1, a 1:1 mixture of ^{15}N-labeled SIP(1−77) and unlabeled Siah-1 at a final protein concentration of 25 μM was prepared in a buffer containing 20 mM Tris-HCl, 25 mM NaCl, and 10 mM BME at pH 7.2. 2D $^{15}N-^{1}H$ HSQC spectra were acquired at 303 K with 128 scans. A similar 1:1 complex was prepared with ^{15}N-labeled SIP and unlabeled Siah-1 at final protein concentrations of 30 μM in a buffer containing 50 mM Tris-HCl, 25 mM NaCl, and 10 mM BME at pH 7.0. For this sample, 2D $^{15}N-^{1}H$ HMQC spectra were acquired at 310 K with 256 scans. This experiment was repeated under identical conditions with a complex containing SIP(74−178) and Siah-1 proteins in a 1:2 molar ratio.

For titrations with Skp1, 100 μM ^{15}N-labeled samples of SIP and SIP(73−229) in 20 mM NaP_i, 50 mM NaCl, and 5 mM DTT at pH 7.0 were titrated with concentrated solutions of Skp1 prepared in an identical buffer. 2D $^{15}N-^{1}H$ HSQC spectra were acquired at 303 K with 32 scans.

Structure Calculations. Input distance constraints for SIP-N were generated from NOESY cross-peak intensities with the upper bounds set to 3.5, 4.5, and 6.0 Å. The φ and ψ angles for the helical regions were restrained to $-65 \pm 25°$ and $-45 \pm 25°$, respectively, based on the $^{3}J_{N\alpha}$ values and CSI analysis within TALOS (*7*). Since residues 56−77 do not have regular secondary structure and are not associated with any long-range NOEs to the remainder of the protein, this region was excluded from the subsequent calculations.

An ensemble of 100 structures was first generated in CYANA (version 1.0.6) (*18*) using 18 restraints per residue (Table 1). SANE (*9*) was used for distance filtering in several iterations of structure-based NOE assignments. The 50 best structures with a target function of less than 1.5e-04 were selected for 3000 steps of restrained energy minimization followed by two rounds of restrained simulated annealing calculations over 20 ps in AMBER version 7.0 (*41*). The final structures were selected on the basis of lowest constraint violation energies and large negative molecular energies. A minimum of 20 structures was found to be adequate to represent the family (*47*). Analysis of the ensemble with PROCHECK_NMR (*25*) revealed more than 98% of the residues in the allowed regions of the Ramachandran plot. The structural coordinates have been deposited in the Protein Data Bank (entry 1YSM) and the chemical shifts in the BioMagResBank (entry 6498).

A homology model of the SIP CS domain was built using the NMR structure of the Sgt1 CS domain (35% identical sequence) as a template in the 3D-PSSM webserver (*23*). The predicted secondary structure agrees with CSI analysis performed with the backbone chemical shifts (BMRB entry 6500) within TALOS.

RESULTS AND DISCUSSION

Structural Characterization of SIP. The structural properties of SIP were investigated by comparing the $^{15}N-^{1}H$ HSQC NMR spectra of the intact protein with those of the isolated domains. To this end, a series of bacterial expression vectors were constructed on the basis of sequence analysis (Figure 1), and the proteins were produced by standard methods. Figure 2 shows the HSQC spectra for residues 1−77, 74−178, and 178−229. The dispersion of NMR resonances clearly shows that the N-terminal and central fragments contain independent folded globular domains, whereas the C-terminal fragment is not folded. Additional spectra were acquired for residues 155−229 and 73−229 (Supporting Information), but the lack of signal dispersion for the C-terminal residues was not affected by extending

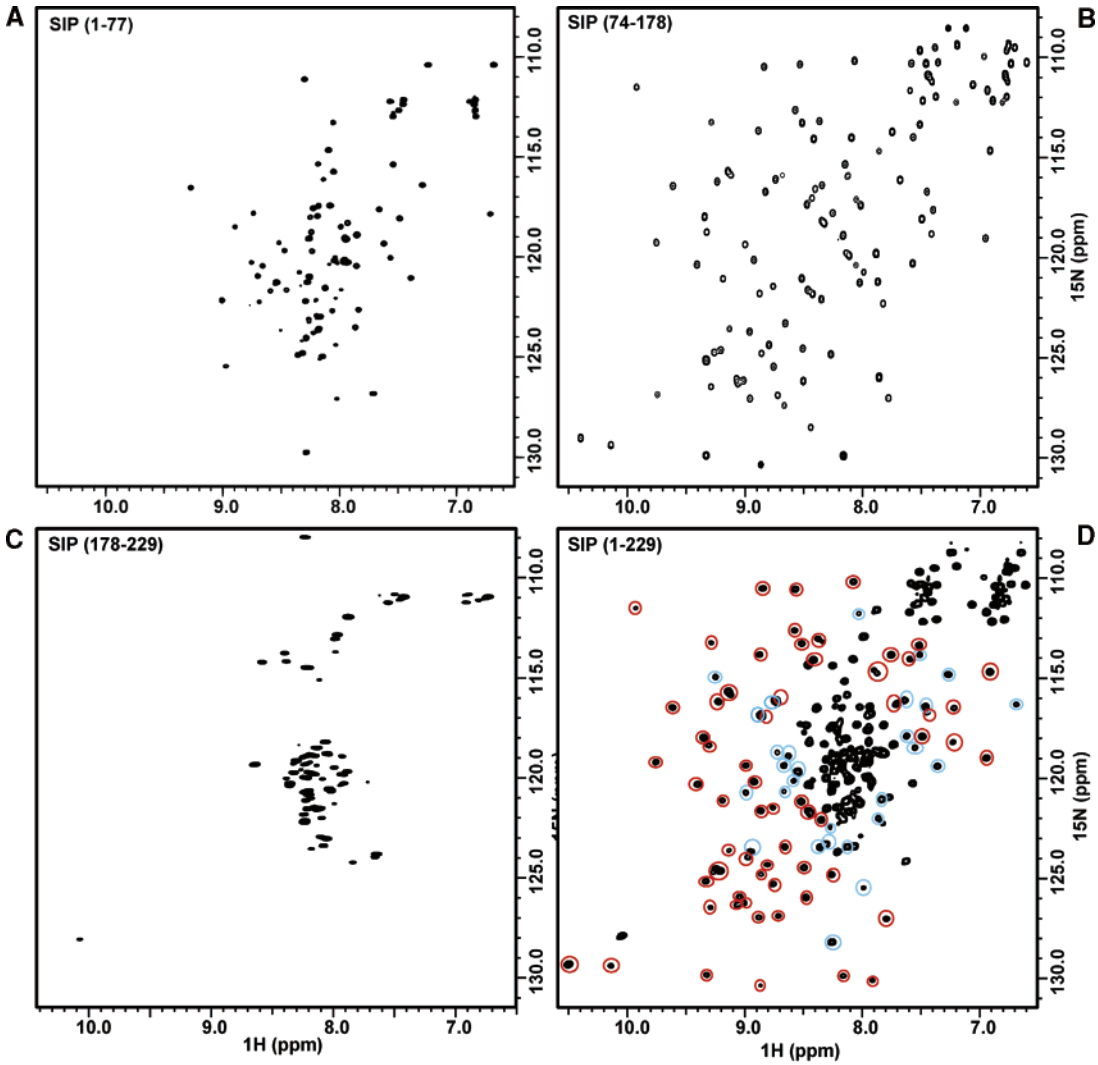

FIGURE 2: SIP has a modular structure. $^{15}N-^{1}H$ HSQC NMR spectra of (A) SIP(1−77), (B) SIP(74−178), (C) SIP(178−229), and (D) the intact SIP protein. All protein samples were prepared in 20 mM NaP_i and 50 mM NaCl buffer at pH 7.0 and 303 K. In the spectrum of the intact protein, blue circles indicate peaks from SIP(1−77) and red circles those from the CS domain. The unmarked peaks represent the signals from SIP(1−77) and SIP(74−178) that are overlapped, as well as those that arise from the poorly structured C-terminal region.

the N-terminus of these constructs. Moreover, the 1:1 correspondence between the cross-peaks observed in the sum of the spectra of the isolated domains of SIP and the spectrum of the intact protein indicates that the two structured domains are independent. Analysis of the corresponding CD spectra indicates the N-terminal fragment contains helical structure, whereas β-sheet structure is present in the central CS-containing fragment. The C-terminal region in isolation or when fused to the CS domain has a small degree of helical structure (*40*). The NMR and CD data are fully consistent with sequence analysis, dividing the protein into N-terminal [SIP(1−77)], central CS [SIP(74−178)], and C-terminal SGS [SIP(152−229)] domains.

To further analyze the structural characteristics of SIP and delineate the correspondence between assignments for functional versus structural domains, sequence-specific resonance assignments were made and structures determined for the N-terminal domain (residues 1−77) and the CS domain (residues 74−178). This analysis was also required for the subsequent structural mapping of the binding sites for Skp1 and Siah-1. Of critical importance, because the domains of SIP are structurally independent, is the fact that the NMR chemical shift assignments and structures of the fragments could be directly transferred to the context of the intact protein.

The three-dimensional structure of the N-terminal domain of SIP could not be predicted on the basis of sequence homology and was therefore determined from first principles using solution NMR spectroscopy. Standard heteronuclear multidimensional NMR experiments were readily carried out with this small protein fragment and yielded a large number of experimental restraints. Table 1 provides a summary of structural statistics. The ensemble of 20 representative conformers of SIP residues 1−50 is shown in stereoview in Figure 3A. The first 47 residues of the domain fold into a helical hairpin domain with a hydrophobic core stabilized by a classic knobs-and-holes arrangement of side chains contributed by the two amphipathic helices (Figure 3B). Interestingly, the helical packing of the side chains revealed heptad repeats of hydrophobic and charged side chains reminiscent of antiparallel coiled-coil domains (*30*). The 30 C-terminal residues corresponding to SIP(48−77) did not form regular secondary structure.

The CS domain of SIP is highly homologous to the CS domain of Sgt1 (34% identical), whose 3D structure has been reported previously (*54*). The backbone chemical shifts for

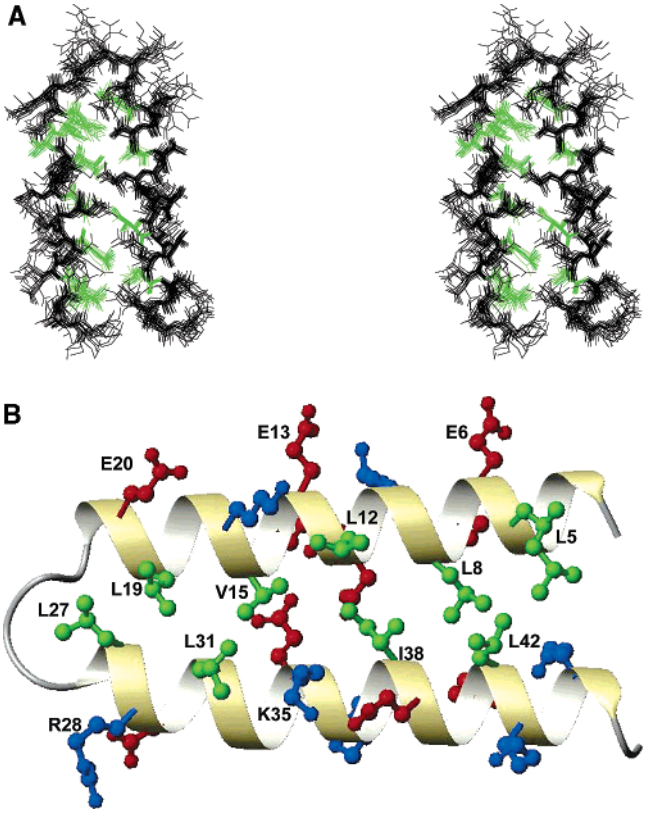

FIGURE 3: Structure of the SIP helical hairpin domain. (A) Stereoview of the ensemble of 20 representative conformers of SIP(1−50). The unstructured C-terminal tail corresponding to residues 51−77 is not shown. The side chains of hydrophobic residues Leu, Val, and Ile are colored green. (B) Single most representative conformer from the NMR ensemble shown as a ribbon diagram. A ball-and-stick representation is used for hydrophobic (green), positively charged (blue), and negatively charged (red) side chains.

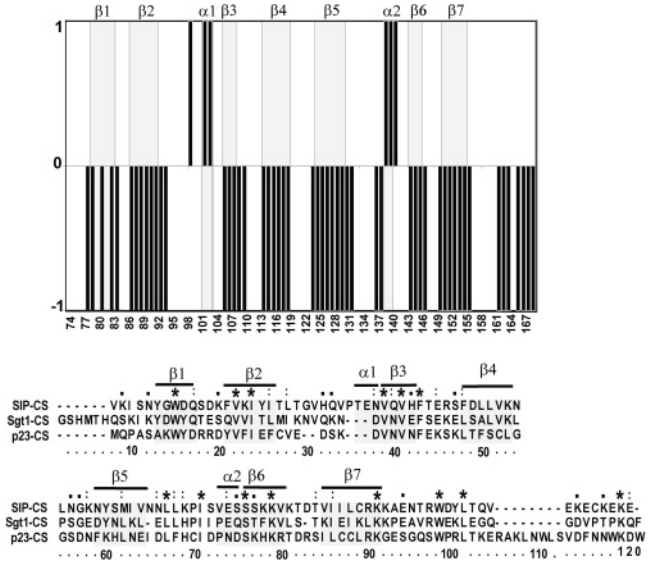

FIGURE 4: Secondary structure of the SIP CS domain. Assignment of secondary structure is based on the chemical shift index calculated with TALOS (*7*). Residues with β-sheet character have a CSI value of −1 and those with α-helical properties a value of 1. Residues predicted to have secondary structure from sequence and structural alignment with the Sgt1 CS domain and p23 are highlighted in gray.

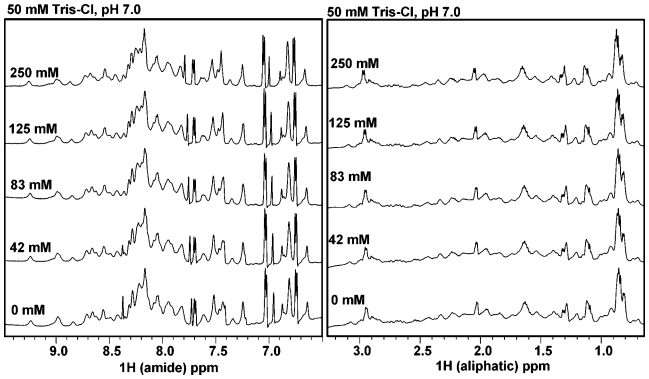

FIGURE 5: 1D proton NMR spectra of 100 μM unlabeled SIP(1−77) dissolved in 50 mM Tris-HCl at pH 7.0 and different NaCl concentrations. The data were acquired on a 600 MHz Bruker spectrometer equipped with a CryoProbe at 300 K. The peaks in the amide and aliphatic regions are plotted in separate panels.

the SIP CS domain were analyzed using TALOS to determine the distribution of elements of regular secondary structure. Figure 4 shows a plot of the chemical shift index for the SIP CS domain, along with a comparison of the predicted secondary structure with that in p23 and the Sgt1 CS domain. Given the similarity in secondary structure and the high level of sequence homology, the SIP CS domain structure could be accurately modeled using the Sgt1 CS domain as a structural template.

Is Native SIP a Dimer? On the basis of two-hybrid assays and gel filtration experiments, Matsuzawa and Reed reported the oligomerization of human SIP protein into higher-order states and identified the 80 N-terminal residues to be critical for self-association (*35*). However, in course of our NMR studies of intact SIP and SIP(1−77), we did not detect oligomeric states as would be manifested by large line widths and poor signal-to-noise ratios. To resolve the apparent discrepancy between the two studies and to confirm the monomeric state of mouse SIP(1−77), a series of one-dimensional proton NMR spectra were acquired at neutral pH and a wide range of salt concentrations (Figure 5). Clearly, there is no change in the line widths of peaks corresponding to amide and aliphatic side chain protons, suggesting the presence of a single species in the buffer used for the studies. Furthermore, a sample consisting of a 1:1 mixture of unlabeled to labeled SIP(1−77) protein was used to probe intermolecular NOEs by filter-edited NMR experiments. But despite our best efforts, we were unable to confirm the presence of oligomeric states spectroscopically.

Our structural characterization suggests that the gel filtration results can be explained by the elongated rodlike shape of SIP with a high degree of anisotropy (1:3, W:L). Our own experience working with the full-length protein shows it is prone to nonspecific aggregation at pH 7.0 ± 2.0, which appears to be mediated by the differences in the charge of the three domains of SIP. The N-terminal region of SIP(1−178) has a high pI of ∼9.0 and is basic, while SIP(178−229) is acidic because of its low pI of ∼4.5. We have made similar observations with other proteins, where acidic and basic domains are linked at neutral pH. Under the conditions at which the NMR experiments were performed, the protein is clearly monomeric. In the absence of a detailed comparative experimental analysis, it is not possible to completely rule out the possibility that differences in the sequence of human and mouse SIP or post-translational modifications give rise to the differences seen between our studies and

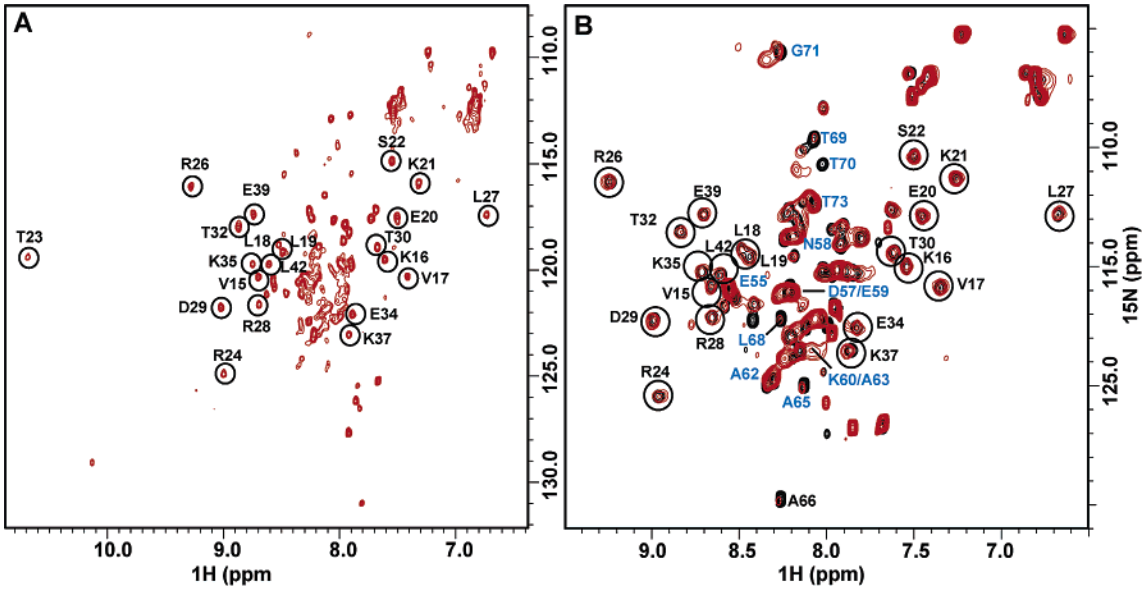

FIGURE 6: Interaction of SIP with Siah-1 monitored by the NMR chemical shift perturbation assay. (A) A 1:1 complex of ^{15}N-labeled SIP and unlabeled Siah(90−282) at pH 7.0 and 310 K. The black circles indicate peaks from the N-terminal helical region of SIP(1−47) that are not perturbed by the interaction between the two proteins. (B) ^{15}N−^{1}H HSQC spectra of free SIP(1−77) (black) and a 1:1 complex of ^{15}N-labeled SIP(1−77) and unlabeled Siah(90−282) (red) at pH 7.0 and 303 K. Residues in the linker region of SIP(48−73) affected by binding of Siah-1 are labeled in blue, while those in the helical hairpin domain that are not perturbed by the interaction between the two proteins are circled in black.

those reported previously. As such, the two proteins are 96% homologous with five differences in the putative oligomerization domain of SIP (residues 1−80). It will be important to determine if the propensity of human SIP to oligomerize is functionally relevant.

Mapping of Protein−Protein Interaction Sites on SIP. The structural analysis of free SIP lays the foundation for analysis of interactions with its two known binding partners in the Siah-1 E3 complex, Skp1 and Siah-1. The approach that was used involved NMR chemical shift mapping, taking advantage of the structures, chemical shift assignments, and modular constructs that were readily available.

SIP and Siah-1 Interactions. Siah-1 is a dimeric protein with a N-terminal RING domain (residues 1−90), tandem cysteine rich zinc-binding domains (residues 90−121 and 122−152), and a TRAF-like domain (residues 153−282) in each subunit (*45*). The entire C-terminal region (residues 90−282) is required for dimerization, and the predominantly electronegative surface of the dimer mediates protein−protein interactions (*10*, *27*, *33*). Although there is significant variation in the amino acid sequence and affinity of Siah-1 binding partners, a common PxAxVxP binding motif has been identified in several cellular binding partners (*20*).

Structural characterization of SIP(1−77) revealed the putative Siah-1 binding region (Pro61−Pro67, PAAVVAP) is part of the unstructured linker region (residues 48−73) that connects the N-terminal helical domain of SIP and the CS domain. NMR titrations of unlabeled Siah(90−282) into ^{15}N-labeled intact SIP resulted in a loss of peak intensity and chemical shift changes for residues (Met46−Gly71) in the linker and, surprisingly, the disappearance of residues from the CS domain (Figure 6A). In contrast, no changes were found in the SIP helical hairpin N-domain or in the SGS domain. These differential effects on residues from different regions of SIP reflect formation of a specific Siah-1 complex. The observed spectral changes can be attributed to a combination of two factors. The weak binding affinity in the range of 1−100 μM (*20*) would be consistent with exchange broadening of NMR signals at a 1:1 molar ratio of the two proteins. Second, the Siah(90−282) dimer complexed with two SIP molecules exceeds 96 kDa, resulting in a loss of signal intensity through slower tumbling times.

The loss of signals from the CS domain was puzzling and prompted further analysis. Although CS domains are known protein interaction modules, it was assumed that binding to Siah-1 occurs at the consensus binding motif in the N-terminal linker. To further delineate the Siah-1 binding site on SIP, additional NMR binding studies were carried out on the isolated N-terminal and CS domains. For the SIP N-terminal region (residues 1−77), differential line broadening, chemical shift perturbations, and a loss in peak intensity of residues located in the linker region are observed as in the intact protein (Figure 6B). In contrast, the NMR signals of the isolated CS domain behaved differently than those in the intact protein, as no perturbations in the CS domain were observed (Supporting Information). This suggests that binding of Siah-1 to SIP is mediated by the consensus motif in the linker. In this model, we reason that the CS domain signals are perturbed by binding of Siah(90−282) not through direct interaction but rather because the motion of the CS domain is sterically restricted by its proximity to the larger Siah(90−282) dimer. As a consequence, the CS domain now tumbles slowly in solution in synchrony with the Siah-1 dimer, and hence, the intensity of its signals is reduced as Siah(90−282) is titrated into the SIP solution. In the presence of the free CS domain, there is no attenuation of signals because there is no direct binding to the CS domain. This interpretation is supported by yeast two-hybrid assays with human SIP(81−228), which showed no interaction with Siah-1 (*35*).

The data we have obtained cannot rule out an alternate explanation, that the interaction of Siah-1 with the CS domain

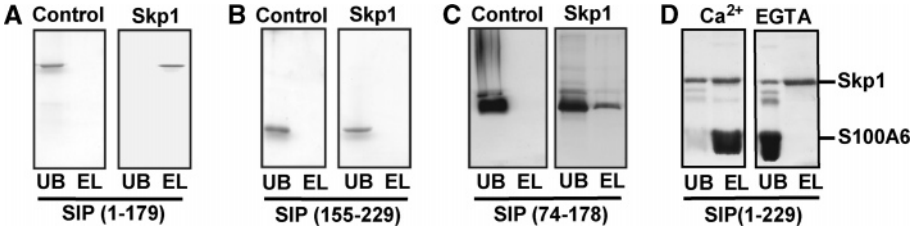

FIGURE 7: Interaction of SIP with Skp1 monitored by affinity chromatography. Skp1-conjugated Sepharose was loaded with SIP fragments corresponding to residues (A) 1−179, (B) 155−229, and (C) 74−178. The bound fraction of the protein was eluted with 0.5 M NaCl. (D) Competitive binding assays with SIP-conjugated Sepharose columns loaded with Skp1 and S100A6 in the presence of Ca^{2+} or EGTA.

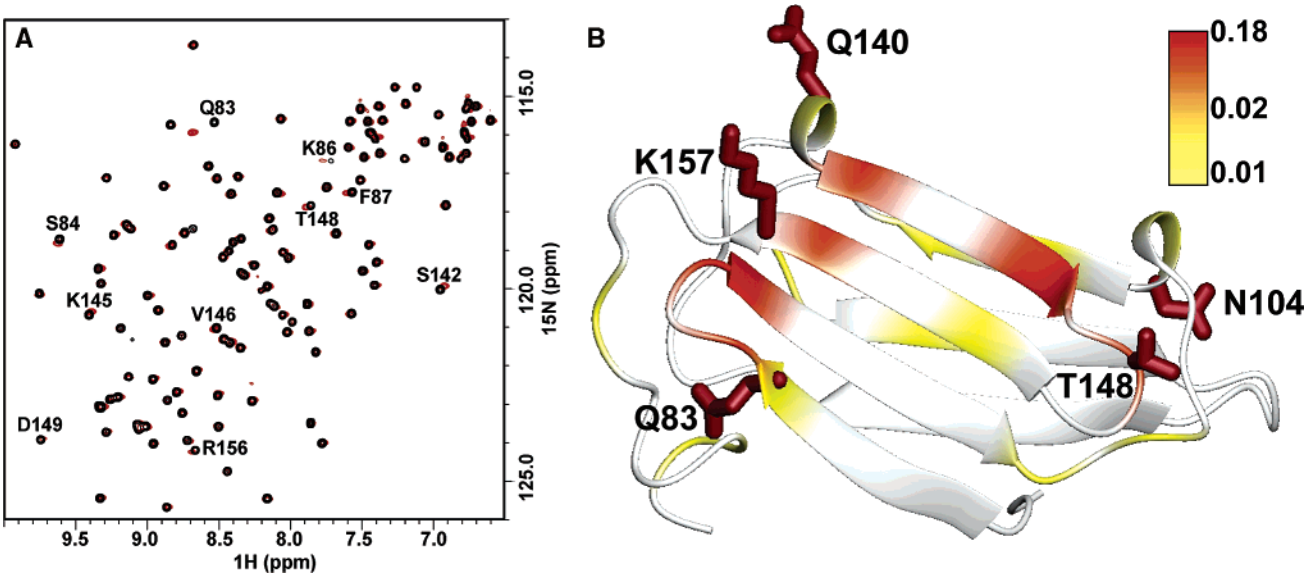

FIGURE 8: Interaction of SIP with Skp1 monitored by the NMR chemical shift perturbation assay. $^{15}N-^{1}H$ HSQC spectra were acquired at pH 7.0 and 303 K. (A) SIP CS domain (black) and 1:2 complex of SIP CS and Skp1 (red). (B) Normalized chemical shift perturbations obtained from panel A mapped on the homology model structure of SIP CS. Chemical shift differences were calculated using the relation $\delta = \sqrt{[(\Delta^{1}H)^2 + (0.5\Delta^{15}N)^2]/2}$. The full range of effects was mapped using the color scheme shown at the right. The side chains are shown and labeled for five conserved polar residues that are important for CS domain function.

is very weak. In this model, the effect on the CS domain resonances in intact SIP arises due to transient, weak *direct* interactions. These interactions are so weak that they fall below the detection limit in the NMR assay with the isolated CS domain. However, when the CS domain is attached to the consensus, higher-affinity interaction site, there is a high local concentration, which in turn leads to a more detectable effect in the intact protein. Mutational analysis of residues at the binding interface should enable differentiation of these two models.

Interactions of SIP with Skp1. Yeast two-hybrid cDNA screening methods were used to identify Skp1, a component of SCF complexes, as a binding partner of SIP(73−229) (*35*). To localize the binding site of Skp1, affinity chromatography experiments were performed with various SIP fragments (Figure 7). These experiments narrowed the interactions to the CS domain. To further characterize the interaction between SIP and Skp1, NMR chemical shift perturbation assays were performed with intact SIP and the isolated domains. The results are consistent with the affinity chromatography experiments, showing interaction exclusively with the CS domain. A combination of binding-induced chemical shift changes and differential broadening of peaks was observed in the spectra of the isolated CS domain (Figure 8) and intact SIP (Supporting Information). Unlike the case for Siah-1, the Skp1-induced perturbations observed for the isolated CS domain were identical to those observed for the intact protein, further supporting our contention of the functional independence of the SIP domains. Working from the resonance assignments, we mapped the chemical shift changes to residues located at one edge of the SIP CS β-sandwich structure and solvent-exposed loops shown in Figure 8. Notably, some of the perturbed residues identified in this study consist of polar side chains that are highly conserved across the CS domain sequences as indicated in Figure 8 (*15*). Five of these positions (Q83, N104, Q140, T148, and K157) have been previously implicated in protein−protein interactions mediated by CS domains in p23 and Hsp20 (*15*).

The binding site for S100A6 had previously been coarsely mapped to SIP(155−229) (*40*). This raised the possibility that the Ca^{2+}-dependent binding of S100A6 could serve to regulate interaction of SIP with Skp1 and the consequent assembly of the Siah-1 E3 ligase. To test this hypothesis, the interactions of SIP, Skp1, and S100A6 were examined in a ternary complex. The strategy involved competitive affinity chromatography experiments (Figure 7). The binding assays indicate that Skp1 and S100 proteins are able to bind to SIP independently and therefore must be interacting at distinctly different sites.

The SIP binding site on Skp1 has been mapped to residues 1−90, which corresponds to the well-known protein−protein

interaction module, the BTB/POZ domain (*35*). This domain has also been shown to be actively involved in interactions with Cullin-1 from the SCF complex (*53*, *55*). Interactions with the F-Box from proteins such as Skp2 (*55*) and β-TrCP1 (*50*) have been mapped to the C-terminal region of Skp1. A similar arrangement is presumably employed in the Siah-1 E3 complex such that the F-Box from Ebi binds in the C-terminal half of Skp1.

Both our results and previous studies (*35*) describe the isolated Skp1 protein as being sufficient for binding SIP. Affinity chromatography results suggest that the interaction is relatively weak. The NMR-based chemical shift perturbations indicate no significant structural changes in the SIP CS domain are induced by the binding of Skp1 (Figure 8). That the interaction is weak is likely to be functionally significant, enabling the rapid release of Skp1 for the formation of other F-Box complexes. However, it is likely that the Ebi F-Box has an allosteric effect on the structure and stability of the interactions between SIP and Skp1. The extensive intermolecular contacts observed in the structure of the F-Box with Skp1 (*50*, *55*) and elongin C (*3*) suggest that the C-terminal helical region of Skp1 may be conformationally heterogeneous in the absence of a binding partner, but that the interaction with the F-Box will induce structure. The $^{15}N-^{1}H$ HSQC spectrum of Skp1 in isolation corroborates this conclusion in that the signals from this region of the protein are poorly dispersed (data not shown). Further studies aimed at investigating the specific effects associated with the formation of the ternary complex are in progress to verify and refine this model.

CONCLUSIONS

Ubiquitination is now widely recognized as a central signaling mechanism in biology. It has become increasingly apparent that a large number of proteins are ubiquitinated at some stage in their lifetime. There is a need to recognize a wide range of proteins to ubiquitinate them, and E3 ubiquitin ligases play a central role in generating this functional diversity.

The multiprotein SCF assemblies are remarkable examples of using a combinatorial approach to achieve a high level of structural and functional diversity. The modular structure of components is vital for creating an adaptable architecture that facilitates the rapid assembly, chemical activity, and subsequent disassembly of the ubiquitination complexes. The adaptable E3 ligase Siah-1 is one example consisting of a tandem RING domain and a substrate-binding domain serving as a scaffold for interactions with a large number of substrates. Additional functional diversity is generated by employing a passive linker to interact with Skp1−F-Box protein subcomplexes.

The accumulated evidence clearly defines multiple roles for SIP in mediating essential protein−protein interactions. The relative independence of the structured modules plays an important role in facilitating the binding of the components of the Siah-1−Skp1−Ebi F-Box complex. The NMR perturbation assays firmly established that Siah-1 interacts with a flexible linker between the helical hairpin domain at the N-termini of SIP and the CS domain. An important outcome of this interaction would be to reduce the conformational entropy in the linker, which will assist in correctly

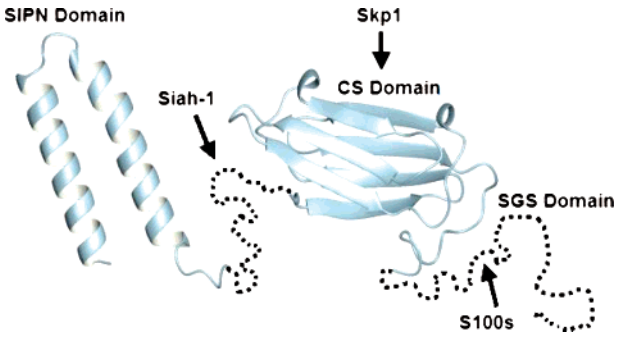

FIGURE 9: Modular structure of SIP. The structured residues (1−47) at the N-terminal part of SIP and the CS domain (74−178) from homology modeling are colored blue. The site for Siah-1 interactions in the unstructured linker (residues 48−73) and the S100 binding site in the unstructured C-terminal region (residues 178−229) are indicated with dashed lines.

orienting Siah-1 with respect to the Skp1−Ebi subcomplex. In contrast, Skp1 appears to engage the SIP CS domain through transient but specific contacts, an interaction that appears not to be extensively coupled to the other domains.

CS domains have been identified in a variety of cochaperone proteins such as p23 and Sgt1. In these systems, Hsp90 is recruited by the CS domain to regulate the formation of macromolecular assemblies (*1*, *22*, *28*, *49*, *54*). For example, Sgt1 recruits Hsp90 to stimulate interactions between Skp1p and the Ctf13 F-box in the CBF3 subcomplex that are essential for formation of the kinetochore in budding yeast (*1*, *24*, *28*, *54*). Similarly, in plant disease resistance, Hsp90 associates with cochaperones RAR1 and Sgt1 to regulate the stability and function of the client protein RPM1 (*21*). On the basis of these similarities, we predict that SIP will bind Hsp90 via the CS domain and serve as a cofactor for stabilizing the interactions with Skp1 and Ebi in the E3 ligase complex.

SIP appears not to engage in specific catalytic activity but is part of a growing family of adaptor proteins that mediate the correct assembly of ubiquitination complexes to achieve functional diversity. Although the β-catenin degradation pathway presents one functional arrangement where SIP links Siah-1 with the Skp1−Ebi subcomplex, SIP could in theory recruit substrates directly. This speculation is supported in part by the example of phyllopod (PHYL), which physically links the E3 ligase SINA (Siah-1 homologue in *Drosophila*) with the transcriptional activator Tramtrack for degradation in the Sevenless pathway (*27*). The parallel between the complexes is intriguing when one considers the fact that PHYL employs a Siah-1 binding motif similar to SIP to bind SINA, but a novel sequence motif to interact with the POZ domain of Tramtrack (*27*). This pairwise interaction appears to be a structural substitute for the interactions between the CS domain of SIP and the POZ domain of Skp1. Although the F-Box protein Ebi is also present in this complex, it does not function in recruiting the substrate Tramtrack. Hence, PHYL combines the functionality of the SIP-Skp1-Ebi complex into a single molecular entity.

The tertiary structure of SIP is reminiscent of beads on a string (Figure 9). The principal role of SIP appears to be bringing various components of the complex into physical proximity, orchestrating the correct distance and orientation of the E2 enzyme and the site on β-catenin for ubiquitination. It is known that the distance between the two reactants is

critically important for achieving a biologically relevant rate of polyubiquitination (*50*). With these and studies from other laboratories, we have begun to piece together critical aspects of the molecular architecture of the Siah-1−Skp1−Ebi ubiquitination complex. Extending these insights to span the entire assembly and understanding the factors important for functional specificity are key areas of future investigation.

ACKNOWLEDGMENT

We thank Accelrys Inc. for beta versions of FELIX software, Dr. Jaison Jacob for help with NMR data acquisition, and Dr. Craig Vanderkooi for helpful comments.

SUPPORTING INFORMATION AVAILABLE

$^{15}N-^{1}H$ spectra of SIP(155−229) and SIP(73−229), $^{15}N-^{1}H$ HMQC spectra of free SIP(74−178) and a 1:2 mixture of ^{15}N-labeled SIP(74−178) and unlabeled Siah(90−282), normalized chemical shift changes obtained from Skp1 titrated into SIP CS (2:1 ratio), and $^{15}N-^{1}H$ HSQC spectra of intact SIP and a 1:2 complex of ^{15}N-labeled SIP and unlabeled Skp1(90−282). This material is available free of charge via the Internet at http://pubs.acs.org.

REFERENCES

1. Bansal, P. K., Abdulle, R., and Kitagawa, K. (2004) Sgt1 associates with Hsp90: An initial step of assembly of the core kinetochore complex, *Mol. Cell. Biol. 24*, 8069−8079.
2. Bax, A., Vuister, G. W., Grzesiek, S., Delaglio, F., Wang, A. C., Tschudin, R., and Zhu, G. (1994) Measurement of Homo- and Heteronuclear J couplings from quantitative J Correlation, *Methods Enzymol. 239*, 79−105.
3. Botuyan, M. V., Koth, C. M., Mer, G., Chakrabartty, A., Conaway, J. W., Conaway, R. C., Edwards, A. M., Arrowsmith, C. H., and Chazin, W. J. (1999) Binding of elongin A or a von Hippel-Lindau peptide stabilizes the structure of yeast elongin C, *Proc. Natl. Acad. Sci. U.S.A. 96*, 9033−9038.
4. Brabletz, T., Jung, A., Dag, S., Hlubek, F., and Kirchner, T. (1999) β-Catenin regulates the expression of the matrix metalloproteinase-7 in human colorectal cancer, *Am. J. Pathol. 155*, 1033−1038.
5. Cavanagh, J., Fairbrother, W. J., Palmer, A. G. I., and Skelton, N. J. (1996) *Protein NMR Spectroscopy: Principles and Practice*, Academic Press, San Diego.
6. Clevers, H., and van de Wetering, M. (1997) TCF/LEF factor earn their wings, *Trends Genet. 13*, 485−489.
7. Cornilescu, G., Delaglio, F., and Bax, A. (1999) Protein backbone angle restraints from searching a database for chemical shift and sequence homology, *J. Biomol. NMR 13*, 289−302.
8. Desterro, J. M., Rodriguez, M. S., and Hay, R. T. (2000) Regulation of transcription factors by protein degradation, *Cell. Mol. Life Sci. 57*, 1207−1219.
9. Duggan, B. M., Legge, G. B., Dyson, H. J., and Wright, P. E. (2001) SANE (Structure Assisted NOE Evaluation): An automated model-based approach for NOE assignment, *J. Biomol. NMR 19*, 321−329.
10. Fanelli, M., Fantozzi, A., De Luca, P., Caprodossi, S., Matsuzawa, S. I., Lazar, M. A., Pelicci, P. G., and Minucci, S. (2003) The coiled-coil domain is the structural determinant for SIAH-mediated degradation of PML and other TRIM proteins by the proteasome, *J. Biol. Chem. 279*, 5374−5379.
11. Filipek, A., Jastrzebska, B., Nowotny, M., and Kuznicki, J. (2002) CacyBP/SIP, a calcyclin and Siah-1-interacting protein, binds EF-hand proteins of the S100 family, *J. Biol. Chem. 277*, 28848−28852.
12. Filipek, A., Jastrzebska, B., Nowotny, M., Kwiatkowska, K., Hetman, M., Surmacz, L., Wyroba, E., and Kuznicki, J. (2002) Ca^{2+}-dependent translocation of the calcyclin-binding protein in neurons and neuroblastoma NB-2a cells, *J. Biol. Chem. 277*, 21103−21109.
13. Filipek, A., and Kuznicki, J. (1998) Molecular cloning and expression of a mouse brain cDNA encoding a novel protein target of calcyclin, *J. Neurochem. 70*, 1793−1798.
14. Fiucci, G., Beaucourt, S., Duflaut, D., Lespagnol, A., Stumptner-Cuvelette, P., Geant, A., Buchwalter, G., Tuynder, M., Susini, L., Lassalle, J. M., Wasylyk, C., Wasylyk, B., Oren, M., Amson, R., and Telerman, A. (2004) Siah-1b is a direct transcriptional target of p53: Identification of the functional p53 responsive element in the siah-1b promoter, *Proc. Natl. Acad. Sci. U.S.A. 101*, 3510−3515.
15. Garcia-Ranea, J. A., Mirey, G., Camonis, J., and Valencia, A. (2002) p23 and Hsp20/α-crystallin proteins define a conserved sequence domain present in other eukaryotic protein families, *FEBS Lett. 529*, 162−167.
16. Grzesiek, S., Kuboniwa, H., Hinck, A. P., and Bax, A. (1995) Multiple-Quantum line narrowing for measurement of Ha-Hb J couplings in isotopically enriched proteins, *J. Am. Chem. Soc. 117*, 5312−5315.
17. He, T. C., Sparks, A. B., Rago, C., Hermeking, H., Zawel, L., da Costa, L. T., Morin, P. J., Vogelstein, B., and Kinzler, K. W. (1998) Identification of c-MYC as a target of the APC pathway, *Science 281*, 1509−1512.
18. Herrmann, T., Guntert, P., and Wuthrich, K. (2002) Protein NMR structure determination with automated NOE assignment using the new software CANDID and the torsion angle dynamics algorithm DYANA, *J. Mol. Biol. 319*, 209−227.
19. Hershko, A., and Ciechanover, A. (1998) The ubiquitin system, *Annu. Rev. Biochem. 67*, 425−479.
20. House, C. M., Frew, I. J., Huang, H. L., Wiche, G., Traficante, N., Nice, E., Catimel, B., and Bowtell, D. D. (2003) A binding motif for Siah ubiquitin ligase, *Proc. Natl. Acad. Sci. U.S.A. 100*, 3101−3106.
21. Hubert, D. A., Tornero, P., Belkhadir, Y., Krishna, P., Takahashi, A., Shirasu, K., and Dangl, J. L. (2003) Cytosolic HSP90 associates with and modulates the *Arabidopsis* RPM1 disease resistance protein, *EMBO J. 22*, 5679−5689.
22. Johnson, J. L., and Toft, D. O. (1995) Binding of p23 and hsp90 during assembly with the progesterone receptor, *Mol. Endocrinol. 9*, 670−678.
23. Kelley, L. A., MacCallum, R. M., and Sternberg, M. J. (2000) Enhanced genome annotation using structural profiles in the program 3D-PSSM, *J. Mol. Biol. 299*, 499−520.
24. Kitagawa, K., Skowyra, D., Elledge, S. J., Harper, J. W., and Hieter, P. (1999) SGT1 encodes an essential component of the yeast kinetochore assembly pathway and a novel subunit of the SCF ubiquitin ligase complex, *Mol. Cell 4*, 21−33.
25. Laskowski, R. A., Rullmannn, J. A., MacArthur, M. W., Kaptein, R., and Thornton, J. M. (1996) AQUA and PROCHECK-NMR: Programs for checking the quality of protein structures solved by NMR, *J. Biomol. NMR 8*, 477−486.
26. Li, S., Li, Y., Carthew, R. W., and Lai, Z. C. (1997) Photoreceptor cell differentiation requires regulated proteolysis of the transcriptional repressor Tramtrack, *Cell 90*, 469−478.
27. Li, S., Xu, C., and Carthew, R. W. (2002) Phyllopod acts as an adaptor protein to link the sina ubiquitin ligase to the substrate protein tramtrack, *Mol. Cell. Biol. 22*, 6854−6865.
28. Lingelbach, L. B., and Kaplan, K. B. (2004) The Interaction between Sgt1p and Skp1p Is Regulated by HSP90 Chaperones and Is Required for Proper CBF3 Assembly, *Mol. Cell. Biol. 24*, 8938−8950.
29. Liu, J., Stevens, J., Rote, C. A., Yost, H. J., Hu, Y., Neufeld, K. L., White, R. L., and Matsunami, N. (2001) Siah-1 mediates a novel β-catenin degradation pathway linking p53 to the *Adenomatous polyposis coli* protein, *Mol. Cell 7*, 927−936.
30. Lupas, A., Van Dyke, M., and Stock, J. (1991) Predicting coiled coils from protein sequences, *Science 252*, 1162−1164.
31. Maeda, A., Yoshida, T., Kusuzaki, K., and Sakai, T. (2002) The characterization of the human Siah-1 promoter(1), *FEBS Lett. 512*, 223−226.
32. Mann, B., Gelos, M., Siedow, A., Hanski, M. L., Gratchev, A., Ilyas, M., Bodmer, W. F., Moyer, M. P., Riecken, E. O., Buhr, H. J., and Hanski, C. (1999) Target genes of β-catenin-T cell-factor/lymphoid-enhancer-factor signaling in human colorectal carcinomas, *Proc. Natl. Acad. Sci. U.S.A. 96*, 1603−1608.
33. Matsuzawa, S., Li, C., Ni, C. Z., Takayama, S., Reed, J. C., and Ely, K. R. (2003) Structural analysis of Siah1 and its interactions with Siah-interacting protein (SIP), *J. Biol. Chem. 278*, 1837−1840.
34. Matsuzawa, S., Takayama, S., Froesch, B. A., Zapata, J. M., and Reed, J. C. (1998) p53-inducible human homologue of *Drosophila* seven in absentia (Siah) inhibits cell growth: Suppression by BAG-1, *EMBO J. 17*, 2736−2747.

35. Matsuzawa, S. I., and Reed, J. C. (2001) Siah-1, SIP, and Ebi collaborate in a novel pathway for β-catenin degradation linked to p53 responses, *Mol. Cell 7*, 915−926.
36. Morin, P. J. (1999) β-Catenin signaling and cancer, *BioEssays 21*, 1021−1030.
37. Muhandiram, D. R., and Kay, L. E. (1994) Gradient-Enhanced Triple-Resonance Three-Dimensional NMR Experiments with Improved Sensitivity, *J. Magn. Reson., Ser. B 103*, 203−216.
38. Naito, M., Katayama, R., Ishioka, T., Suga, A., Takubo, K., Nanjo, M., Hashimoto, C., Taira, M., Takada, S., Takada, R., Kitagawa, M., Matsuzawa, S., Reed, J. C., and Tsuruo, T. (2004) Cellular FLIP inhibits β-catenin ubiquitylation and enhances Wnt signaling, *Mol. Cell. Biol. 24*, 8418−8427.
39. Neri, D., Szyperski, T., Otting, G., Senn, H., and Wuthrich, K. (1989) Stereospecific nuclear magnetic resonance assignments of the methyl groups of valine and leucine in the DNA-binding domain of the 434 repressor by biosynthetically directed fractional ^{13}C labeling, *Biochemistry 28*, 7510−7516.
40. Nowotny, M., Bhattacharya, S., Filipek, A., Krezel, A. M., Chazin, W., and Kuznicki, J. (2000) Characterization of the interaction of calcyclin (S100A6) and calcyclin-binding protein, *J. Biol. Chem. 275*, 31178−31182.
41. Pearlman, D. A., Case, D. A., Caldwell, J. C., Seibel, G. L., Singh, U. C., Weiner, P., and Kollman, P. A. (1991) *Amber*, University of California, San Francisco.
42. Peifer, M., and Polakis, P. (2000) Wnt signaling in oncogenesis and embryogenesis: A look outside the nucleus, *Science 287*, 1606−1609.
43. Pickart, C. M. (2001) Mechanisms underlying ubiquitination, *Annu. Rev. Biochem. 70*, 503−533.
44. Polakis, P. (1999) The oncogenic activation of β-catenin, *Curr. Opin. Genet. Dev. 9*, 15−21.
45. Polekhina, G., House, C. M., Traficante, N., Mackay, J. P., Relaix, F., Sassoon, D. A., Parker, M. W., and Bowtell, D. D. (2002) Siah ubiquitin ligase is structurally related to TRAF and modulates TNF-α signaling, *Nat. Struct. Biol. 9*, 68−75.
46. Sattler, M., Schleucher, J., and Greisinger, C. (1999) Heteronuclear multidimensional NMR experiments for the structure determination of proteins in solution employing pulse field gradients, *Prog. NMR Spectrosc. 34*, 93−158.
47. Smith, J., Paloma, L. G., Case, D. A., and Chazin, W. J. (1996) Molecular dynamics docking driven by NMR derived restraints to determine the structure of the calicheamicin γ1I oligosaccharide domain complexed to duplex DNA. *Magn. Reson. Chem. 34*, 147−155.
48. Tetsu, O., and McCormick, F. (1999) β-Catenin regulates expression of cyclin D1 in colon carcinoma cells, *Nature 398*, 422−426.
49. Weaver, A. J., Sullivan, W. P., Felts, S. J., Owen, B. A., and Toft, D. O. (2000) Crystal structure and activity of human p23, a heat shock protein 90 co-chaperone, *J. Biol. Chem. 275*, 23045−23052.
50. Wu, G., Xu, G., Schulman, B. A., Jeffrey, P. D., Harper, J. W., and Pavletich, N. P. (2003) Structure of a β-TrCP1-Skp1-β-catenin complex: Destruction motif binding and lysine specificity of the SCF (β-TrCP1) ubiquitin ligase, *Mol. Cell 11*, 1445−1456.
51. Wu, J., Tan, X., Peng, X., Yuan, J., and Qiang, B. (2003) Translocation and phosphorylation of calcyclin binding protein during retinoic acid-induced neuronal differentiation of neuroblastoma SH-SY5Y cells, *J. Biochem. Mol. Biol. 36*, 354−358.
52. Xiao, J. H., Ghosn, C., Hinchman, C., Forbes, C., Wang, J., Snider, N., Cordrey, A., Zhao, Y., and Chandraratna, R. A. (2003) *Adenomatous polyposis coli* (APC)-independent regulation of β-catenin degradation via a retinoid X receptor-mediated pathway, *J. Biol. Chem. 278*, 29954−29962.
53. Yan, Q., Kamura, T., Cai, Y., Jin, J., Ivan, M., Mushegian, A., Conaway, R. C., and Conaway, J. W. (2004) Identification of elongin C and skp1 sequences that determine cullin selection, *J. Biol. Chem. 279*, 43019−43026.
54. Lee, Y.-T., Jacob, J., Michowski, W., Nowontny, M., Kuznichi, J., and Chazin, W. J. (2004) Human Sgt1 binds HSP90 through the CHORD-Sgt1 domain and not the tetratricopeptide repeat domain, *J. Biol. Chem. 279*, 16511−16517.
55. Zheng, N., Schulman, B. A., Song, L., Miller, J. J., Jeffrey, P. D., Wang, P., Chu, C., Koepp, D. M., Elledge, S. J., Pagano, M., Conaway, R. C., Conaway, J. W., Harper, J. W., and Pavletich, N. P. (2002) Structure of the Cul1-Rbx1-Skp1-F box Skp2 SCF ubiquitin ligase complex, *Nature 416*, 703−709.

BI0502689